A&A 525, A132 (2011)
DOI: 10.1051/0004-6361/201015312

Astronomy & Astrophysics

The HII region G35.673-00.847: another case of triggered star formation?

S. Paron[1,2], A. Petriella[1], and M. E. Ortega[1]

[1] Instituto de Astronomía y Física del Espacio (IAFE), CC 67, Suc. 28, 1428 Buenos Aires, Argentina
e-mail: sparon@iafe.uba.ar
[2] FADU – Universidad de Buenos Aires, Argentina

Received 30 June 2010 / Accepted 18 October 2010

ABSTRACT

Aims. As part of a systematic study that we are performing to increase the observational evidence of triggered star formation in the surroundings of HII regions, we analyze the ISM around the HII region G35.673-00.847, a poorly studied source.
Methods. Using data from the large-scale surveys Two Micron All Sky Survey, Galactic Legacy Infrared Mid-Plane Survey Extraordinaire (GLIMPSE), MIPSGAL, Galactic Ring Survey (GRS), VLA Galactic Plane Survey (VGPS), and NRAO VLA Sky Survey (NVSS), we performed a multiwavelength study of G35.673-00.847 and its surroundings.
Results. The mid-IR emission shows that G35.673-00.847 has an almost semi-ring like shape with a cut towards the galactic west. The radius of this semi-ring is about 1.′5 (~1.6 pc, at the distance of ~3.7 kpc). The distance was estimated from an HI absorption study and the analysis of the molecular gas. We find a molecular shell composed of several clumps distributed around the HII region, suggesting that its expansion is collecting the surrounding material. We identify several YSO candidates across the molecular shell. Finally, comparing the HII region dynamical age and the fragmentation time of the molecular shell, we discard the so-called collect and collapse as being the mechanism responsible for the YSO formation, suggesting that other processes such as radiative-driven implosion and/or small-scale Jeans gravitational instabilities operate.

Key words. HII regions – ISM: clouds – stars: formation

1. Introduction

In the past few years, the Galactic Legacy Infrared Mid-Plane Survey Extraordinaire (GLIMPSE) performed with data obtained from the *Spitzer* Space Telescope has been a very useful tool for studying the Galactic IR emission with unprecedented quality and resolution, and still remains so. Using these mid-IR data, it is possible for instance, to clearly identify the photodissociation regions (PDRs) surrounding HII regions. Thus, from a multiwavelength analysis we can study the interaction between the HII region and the surrounding interstellar medium (ISM) and identify triggered star formation. One of the triggered processes that has been widely studied in HII region borders is the "collect and collapse", which was originally proposed by Elmegreen & Lada (1977). This process occurs during the supersonic expansion of an HII region when a dense layer of material is collected between the ionization and the shock fronts. When this layer fragments into massive condensations that can then collapse to promote the formation of new massive stars and/or clusters. Observational studies have found evidence that this mechanism is taking place in several HII regions (see e.g. Petriella et al. 2010; Pomarès et al. 2009; Zavagno et al. 2007, and references therein).

G35.673-00.847 (hereafter G35.6) is a poorly studied HII region. The source was cataloged in the HII region catalogue of Lockman (1989), who obtained a recombination line at $v_{\rm LSR} \sim 60$ km s^{-1}. According to the IRAS Point Source Catalog, G35.6 coincides with the source IRAS 18569+0159. In the NRAO VLA Sky Survey (NVSS), Condon et al. (1998) identified two radio sources, NVSS 185929+020334 and 185938+020012, towards this region.

This work is part of a systematic study that we are performing to increase the observational evidence of triggered star formation in the surroundings of HII regions. We present a molecular and near- and mid-IR study of the environment that surrounds the HII region G35.6 to explore the ISM around it, and look for signatures of star formation.

2. Data

We analyzed data extracted from the four large-scale surveys Two Micron All Sky Survey (2MASS)[1], Galactic Legacy Infrared Mid-Plane Survey Extraordinaire (GLIMPSE), MIPSGAL, and GRS[2].

GLIMPSE is a mid-infrared survey of the inner Galaxy performed using the *Spitzer* Space Telescope. We used the mosaicked images from GLIMPSE and the GLIMPSE Point-Source Catalog (GPSC) acquired by *Spitzer*-IRAC (3.6, 4.5, 5.8 and 8 μm). IRAC has an angular resolution of between 1.″5 and 1.″9 (see Fazio et al. 2004; Werner et al. 2004). MIPSGAL is a survey of the same region as GLIMPSE, using MIPS instrument (24 and 70 μm) on *Spitzer*. The MIPSGAL resolution at 24 μm is 6″. The GRS was performed by Boston University and the Five College Radio Astronomy Observatory (FCRAO). The survey maps the Galactic ring in the ^{13}CO $J = 1$–0 line with an angular and spectral resolution of 46″ and 0.2 km s^{-1}, respectively

[1] 2MASS is a joint project of the University of Massachusetts and the Infrared Processing and Analysis Center/California Institute of Technology, funded by the National Aeronautics and Space Administration and the National Science Foundation.
[2] Galactic Ring Survey (Jackson et al. 2006).

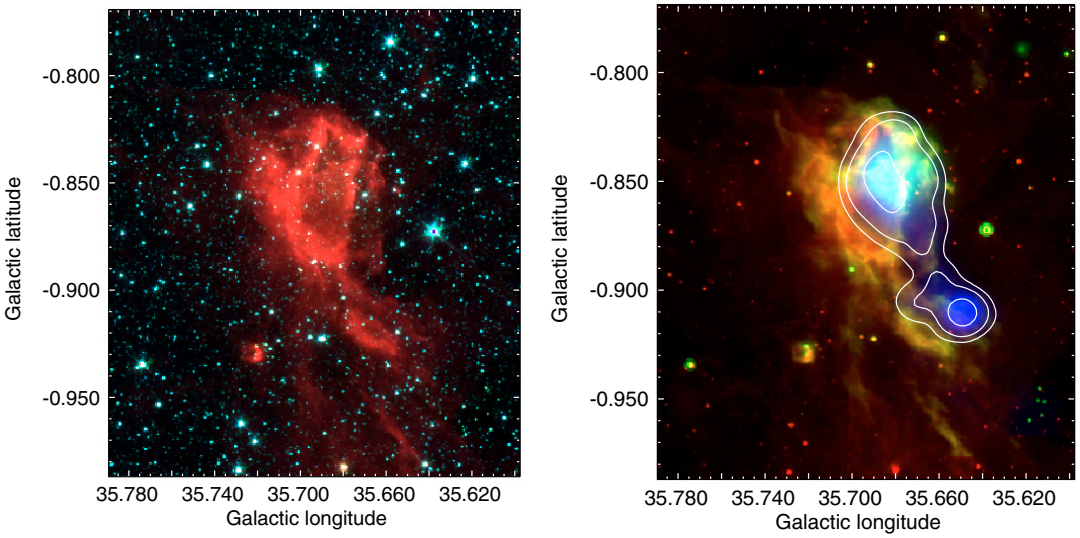

Fig. 1. *Left*: *Spitzer*-IRAC three-color image (3.6 μm = blue, 4.5 μm = green, and 8 μm = red). *Right*: color composite image where the *Spitzer*-IRAC 8 μm emission is displayed in red, the *Spitzer*-MIPSGAL emission at 24 μm is shown in green, and the NVSS radio continuum emission at 20 cm is presented in blue and emphasized by white contours with levels of 2.5, 6, and 20 mJy beam^{-1}. The $\sigma_{\rm rms}$ of the NVSS data is 0.45 mJy beam^{-1}.

(see Jackson et al. 2006). The observations were performed in both position-switching and on-the-fly mapping modes, achieving an angular sampling of 22″.

In addition we used HI data with an angular resolution of ∼1′ extracted from the VLA Galactic Plane Survey (VGPS; Stil et al. 2006) and radio continuum data extracted from the NRAO VLA Sky Survey (NVSS) with an angular resolution of ∼45″ (Condon et al. 1998).

3. Presentation of G35.673-00.847 (G35.6)

Figure 1 shows two composite three-color images of G35.6. The left image displays three *Spitzer*-IRAC bands: 3.6 μm (in blue), 4.5 μm (in green), and 8 μm (in red). The right image shows the *Spitzer*-IRAC emission at 8 μm (in red), the *Spitzer*-MIPSGAL emission at 24 μm (in green), and the NVSS radio continuum emission at 20 cm (in blue and emphasized with white contours). Both figures clearly show the PDR visible in the 8 μm emission, which originates mainly in the polycyclic aromatic hydrocarbons (PAHs). The PAH emission delineates the HII region boundaries because these large molecules are destroyed inside the ionized region, but are excited in the PDR by the radiation leaking from the HII region (Pomarès et al. 2009). The 24 μm emission reveals the presence of hot dust, and the radio continuum emission shows two sources, one related to G35.6, probably due to its ionized gas, and another lying towards the south. These sources are NVSS 185929+020334 and 185938+020012, respectively (Condon et al. 1998). The PAH emission shows that G35.6 has an almost semi-ring like shape with a cut towards the Galactic west. The radius of this semi-ring is about 1.′5. Extending towards the south is another visible PDR, which can be related to the radio continuum source NVSS 185938+020012. On the other hand, a little bubble is present in the field, at $l = 35.^{\circ}722$, $b = -0.^{\circ}928$. The emission at 8 μm and 24 μm, indicating that PAH and hot dust exist towards this bubble, suggests that it could be a young HII region.

4. Distance

G35.6 exhibits a radio recombination line at $v_{\rm LSR} \sim 60$ km s^{-1} (Lockman 1989), which, by applying the flat Galactic rotation curve of Fich et al. (1989) that assumes circular rotation around the Galactic center, gives the possible kinematic distances of ∼4.0 or ∼9.8 kpc. This ambiguity arises because we are studying a region in the first Galactic quadrant, where a given velocity may be associated with two possible distances. Using HI data, we performed an absorption study towards the radio sources G35.6 (NVSS 185929+020334) and NVSS 185938+020012. Figure 2 shows the HI spectra towards both sources. The HI emission obtained over the source (the On position: a beam over the radio maximum of the source) is presented in red, in blue we present the average HI emission taken from four positions separated approximately by a beam from the source in the direction of the four Galactic cardinal points (the Off position), and the subtraction between them is presented in black, which has a 3σ uncertainty of ∼10 K. The figure shows that both sources have similar HI absorption features, suggesting that they are located at the same distance. The last absorption feature appears at $v \sim 61$ km s^{-1}, in coincidence with the G35.6 recombination line (Lockman 1989). Taking into account that the tangent point (at $v \sim 89.7$ km s^{-1}) does not exhibit any absorption, following Kolpak et al. (2003), we favour the near kinematic distance.

5. Molecular analysis

We analyze the whole ^{13}CO $J = 1$–0 data cube and find some interesting molecular structures between 47 and 60 km s^{-1}. Figure 3 displays the integrated velocity channel maps of the ^{13}CO $J = 1$–0 emission every ∼1 km s^{-1}, showing the kinematical and morphological structure of a molecular cloud probably related to the HII region G35.6. Between ∼48 and 51 km s^{-1}, a molecular structure appears delineating the PDR that extends to the south. No molecular gas is observed between 51 and 54 km s^{-1} (this velocity interval is not shown in Fig. 3). Finally, between 54 and 59 km s^{-1}, several molecular clumps appear

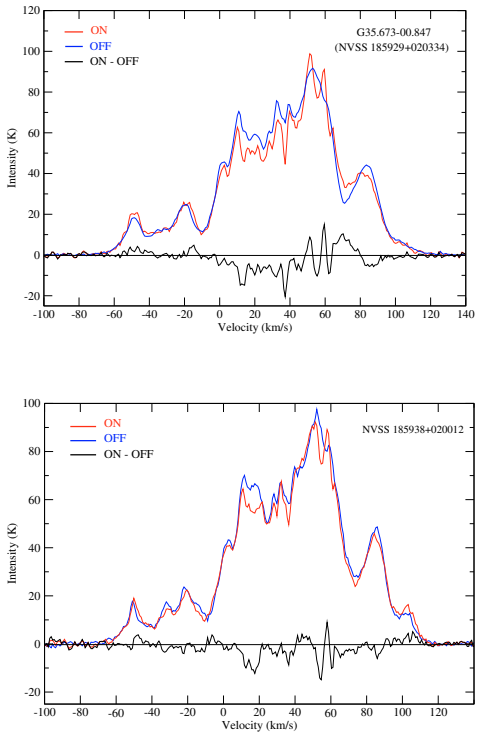

Fig. 2. *Up*: HI spectra obtained towards the source G35.6 (NVSS 185929+020334). *Bottom*: HI spectra obtained towards the source NVSS 185938+020012. The spectra obtained towards the sources (the On position) are presented in red, and in blue we present the averaged HI emission taken from four positions separated approximately by a beam from the source in the direction of the four Galactic cardinal points (the Off position), and the subtractions between them are presented in black. The 3σ uncertainty in the subtraction is ∼10 K.

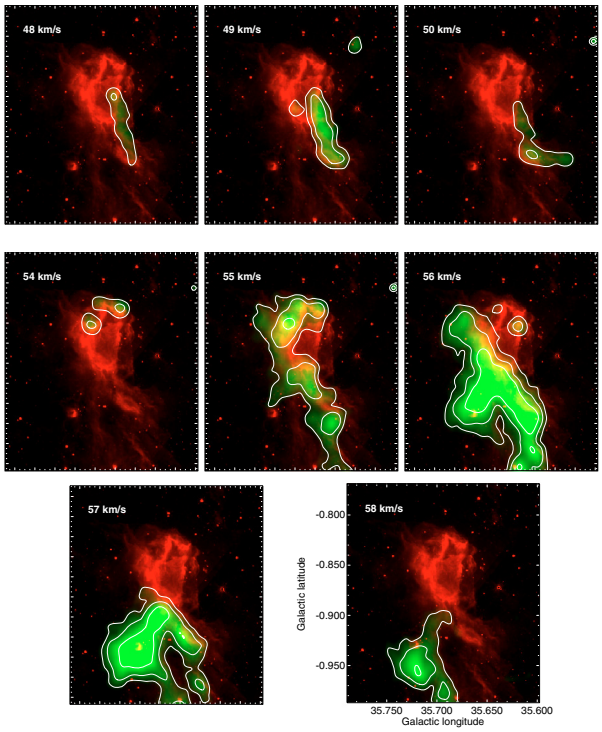

Fig. 3. Integrated velocity channel maps of the ^{13}CO J = 1–0 emission (in green) every ∼1 km s^{-1} in two velocity intervals: from ∼48 to 51 km s^{-1} (shown in the first three panels) and from ∼54 to 59 km s^{-1} (shown in the remaining panels). The contour levels of the ^{13}CO J = 1–0 emission are 1, 2 and 4 K km s^{-1}. Red is the 8 μm emission.

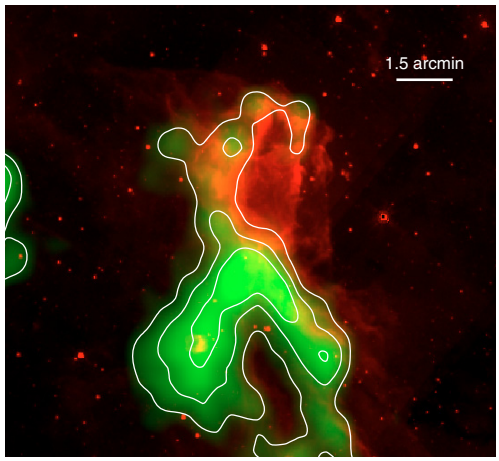

Fig. 4. ^{13}CO J = 1–0 emission (in green) integrated between 53 and 61 km s^{-1}. The contour levels of the ^{13}CO J = 1–0 emission are 4.5, 8 and 12 K km s^{-1}. Red is the 8 μm emission.

distributed over the borders of G35.6 and the southern PDR, which may indicate that the collect and collapse process could be taking place in this region. As Deharveng et al. (2005) point out, the presence of a dense molecular shell surrounding the ionized gas of an HII region, or massive fragments regularly spaced along the ionization front, may be indicative of the collect and collapse mechanism. Figure 4 shows the ^{13}CO J = 1–0 emission integrated between 53 and 61 km s^{-1} (in green) over the 8 μm emission (in red). The very good correspondence between the eastern HII region border, traced by the IR emission, and the molecular gas, strongly suggests that the observed molecular shell has been swept and shaped by the expansion of G35.6. The central velocity of the molecular gas is ∼57 km s^{-1}, which infers a kinematic distance of either 3.7 or 10.1 kpc. According to the study presented in Sect. 4, we favour the nearest one. Taking into account that the ionized gas may be moving away from the molecular material, we use the central velocity of the molecular gas to adopt 3.7 kpc as the distance of the whole complex.

To estimate the mass and density of the described molecular shell, we assume LTE, an excitation temperature of 20 K, a distance of 3.7 kpc, and that the ^{13}CO emission is optically thin. From the standard LTE equations, we obtain a N(^{13}CO) $\sim 3\times10^{16}$ cm^{-2}, and using the relation $N(H_2)/N(^{13}CO) \sim 5\times10^5$ (e.g. Simon et al. 2001) we obtain a molecular mass and a density of $\sim 1.5\times10^4$ $M_\odot$ and $\sim 1\times10^4$ cm^{-3}, respectively. The integration was performed over all the observed positions within the 4.5 K km s^{-1} contour level shown in Fig. 4, following the shell geometry in the 55 km s^{-1} channel map in Fig. 3, i.e., the molecular condensation extending towards the southeast was not considered. To calculate the volume of the molecular shell, we assume a length along the line of sight of ∼1′ (∼1.1 pc at the distance of 3.7 kpc), which is approximately the average of the shell width seen in the plane of the sky (see the 55 km s^{-1} channel map in Fig. 3). On the other hand, we note that the little bubble described in Sect. 3, which is probably a young HII region, is likely to be embedded in this molecular condensation, which appears to be active in star formation.

Table 1. Exciting star candidates in regions R1 and R2.

#	2MASS Designation	J	H	K	A_v	M_J	M_H	M_K	O-type star
					R1				
1	J18593297+0202530	11.92	11.52	11.40	4.18	–2.10	–2.05	–1.91	–
2	J18593204+0204495	16.67	13.34	11.69	30.26	–4.70	–4.80	–4.54	*yes*
3	J18592664+0204362	13.90	10.54	8.86	30.61	–7.58	–7.66	–7.41	–
4	J18593563+0203404	15.05	12.25	10.88	25.44	–4.97	–5.05	–4.81	*yes*
5	J18593189+0203454	14.66	12.11	11.01	22.12	–4.42	–4.60	–4.31	*yes*
6	J18592786+0203057	14.14	11.88	10.92	19.58	–4.23	–4.39	–4.11	*yes*
7	J18593076+0205225	11.11	10.60	10.52	4.31	–2.95	–2.99	–2.80	–
8	J18592979+0202149	13.35	11.05	10.05	20.17	–5.18	–5.32	–5.05	–
9	J18593057+0202486	13.28	10.70	9.53	22.81	–6.00	–6.13	–5.87	–
10	J18592697+0202073	12.66	10.11	8.89	23.09	–6.69	-6.77	–6.53	–
11	J18593472+0204518	16.34	13.32	11.88	27.07	–4.13	–4.26	–3.99	*yes*
12	J18592785+0203304	11.69	10.30	9.56	13.83	–5.05	–4.96	–4.83	*yes*
13	J18593016+0204431	13.84	10.65	8.90	30.39	–7.57	–7.51	–7.35	–
14	J18593041+0202363	14.38	12.47	11.64	16.95	–3.24	-3.34	-3.10	*yes*
15	J18592897+0202470	11.54	9.09	7.87	22.60	–7.67	–7.71	–7.50	–
					R2				
16	J18593584+0200579	14.35	12.37	11.51	17.50	–3.43	-3.53	–3.29	*yes*
17	J18593743+0200411	14.07	11.69	10.58	21.40	–4.81	–4.90	–4.66	*yes*
18	J18593556+0200488	13.81	11.97	11.25	15.70	–3.46	–3.62	–3.35	*yes*
19	J18594015+0200255	15.76	12.94	11.67	24.73	–4.06	–4.23	–3.94	*yes*
20	J18593887+0200288	15.20	12.82	11.71	21.40	–3.68	–3.77	–3.53	*yes*
21	J18593725+0201066	15.22	13.21	12.25	18.47	–2.83	–2.86	–2.66	–

Notes. The sources number correspond to the numeration in Fig. 5.

6. Exciting stars

No exciting star of the HII region G35.6 can be found in the literature. In this work, we provide indirect evidence of the location and properties of the exciting star(s) of the region.

The first piece of information is given by the radio continuum emission of G35.6, which allow us to derive the expected spectral type of the exciting star. The number of UV ionizing photons needed to keep an HII region ionized is given by $N_{\rm uv} = 0.76 \times 10^{47} T_4^{-0.45} \nu_{\rm GHz}^{0.1} S_\nu D_{\rm kpc}^2$ (Chaisson 1976), where T_4 is the electron temperature in units of 10^4 K, $D_{\rm kpc}$ the distance in kpc, $\nu_{\rm GHz}$ the frequency in GHz, and S_ν the measured total flux density in Jy. Assuming an electron temperature of $T = 10^4$ K, a distance of 3.7 kpc, and using a total flux density of 0.86 Jy at 2.7 GHz for G35.6 (Reich et al. 1984) and a total flux density of 0.053 Jy at 1.4 GHz for NVSS 185938+020012 (Condon et al. 1998), the total amount of ionizing photons needed to keep these sources ionized turns out to be about $N_{\rm uv} = 1.0 \times 10^{48}$ ph s^{-1} and $N_{\rm uv} = 0.6 \times 10^{47}$ ph s^{-1}, respectively. It is well established that part of the UV radiation can be dissipated in heating the dust. Inoue (2001) and Inoue et al. (2001), indeed demonstrated that typically only half of the Lyman continuum photons from the central source in a Galactic HII region ionizes neutral hydrogen, the remainder being absorbed by dust grains within the ionized region. We take this into account, consider errors of about ten percent in both the distance and the radio continuum flux at 2.7 GHz, and base on the ionizing fluxes for massive stars given by Martins et al. (2005) to estimate the spectral type of the ionizing star of G35.6 to be between O7.5V and O9V.

In addition we perform a photometric study of the infrared point sources in the region based on the GLIMPSE I Spring′07 and the 2MASS All-Sky Point Source Catalogs. Only sources with detections in the four *Spitzer*-IRAC bands and the three 2MASS bands were considered. We find 30 and 8 sources towards both the HII region G35.6 (R1 in Fig. 5) and the source NVSS 185938+020012 (R2 in Fig. 5), respectively. To examine the evolutionary stage of the infrared point sources, we analyze their location in a color–color IRAC diagram. Following Allen et al. (2004) color criteria, we found 15 and 6 sources in R1 and R2, respectively, which can be classified as main sequence stars (Class III). Table 1 presents these sources with their 2MASS designation (Col. 2), apparent *JHK* magnitudes (Cols. 3–5), estimated extinctions (Col. 6), calculated absolute *JHK* magnitudes (Cols. 7–9), and indication whether their derived spectral type coincides with an O-type in Col. 10. The errors in the estimated

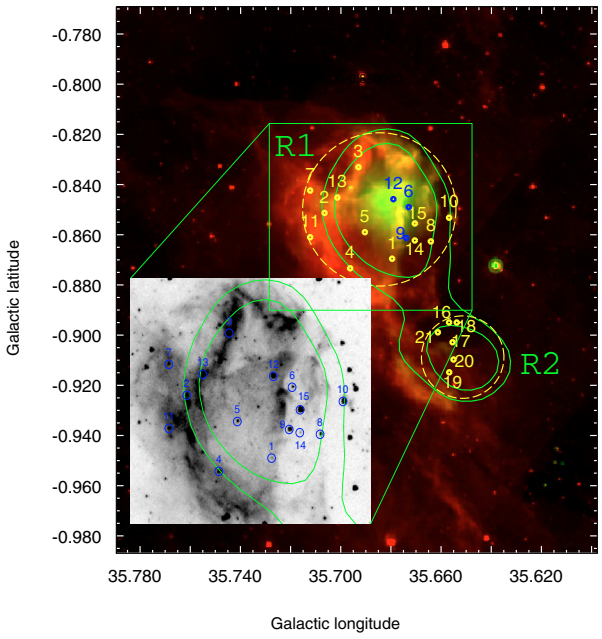

Fig. 5. *Spitzer*-IRAC two-color image (8 μm = red and 24 μm = green). The green contours represent the radio continuum emission at 20 cm. The crosses show the location of the main sequence star candidates in R1 and R2 (dashed circles).

extinctions and the calculated absolute *JHK* magnitudes are below 20% and 30%, respectively. The sources are labeled according to Fig. 5, which displays their location in a two-color image, where the 8 μm and 24 μm emissions are displayed in red and green, respectively. The green contours delineate the radio continuum emission at 20 cm. To search for O-type stars (probably responsible for ionizing the surrounding gas), we use the *J*, *H*, and *K* apparent magnitudes obtained from the 2MASS Point Source Catalog to derive the absolute *JHK* magnitudes. To perform that, we assume a distance of about 3.7 kpc and obtain the extinction for each source from the *(J-H)* and *(H-K)* colors. We assume the interstellar reddening law of Rieke & Lebofsky (1985) ($A_J/A_V = 0.282$, A_H/A_V=0.175, and $A_K/A_V = 0.112$) and the intrinsic colors $(J-H)_0$ and $(H-K)_0$ obtained from Martins & Plez (2006). By comparing the derived absolute magnitudes with those tabulated by Martins & Plez (2006), we find that seven sources in region 1, #2, #4, #5, #6, #11, #12, and #14, and five sources in region 2, #16, #17, #18, #19, and #20, have absolute *JHK* magnitudes that agree with those of an O-type star (see Table 1).

Finally, taking into account that the exciting star candidates are expected to be in a PAH hole, we exclude sources #2, #4, and #11 as the responsible of generate G35.6. The rest of the exciting star candidates, sources #5, #6, #12, and #14, are located in projection within the radio continuum and 24 μm emissions; among them, sources #6 and #12 are located close to the maximum of the 24 μm emission as expected for an exciting star. On the other hand, as can be seen in Fig. 5, source #6 is located in a hole of the 5.8 μm emission (see zoom of the region in the figure). It is well known that the exciting star(s) of an HII region generates a cavity of dust and gas because of the action of the radiation pressure on the dust grains (Gail & Sedlmayr 1979), which suggests that source #6 is the more likely exciting-star candidate of G35.6. On the other hand, using the same assumptions as for R1, we found that based on the radio continuum flux at 1.4 GHz in R2, the exciting stars of NVSS 185938+020012 would be later than an O9.5V star. The later spectral type stars found in R2 could be the sources #16 and #18.

It would be very useful to have UBV fluxes to perform more accurate photometry and identify beyond doubt the exciting stars, although these fluxes are very difficult to obtain because of the interstellar absorption towards this region of the Galaxy.

7. Star formation

In Sect. 5, we show that the HII region G35.6 is evolving and affecting a molecular cloud, presenting an excellent scenario for probing triggered star formation. In this section, we look for young stellar objects (YSOs) around G35.6. YSOs are generally classified according to their evolutionary stage: class I are the youngest sources embedded in dense envelopes of gas and dust, and class II are sources whose emission originates mainly in the accretion disk around the central protostar. In both cases, a YSO exhibits an infrared excess that cannot be attributed to the scattering and absorption of the ISM along the line of sight. In contrast, this infrared excess is mainly caused by the envelope and/or the disk of dust around the central protostar. In other words, YSOs are intrinsically red sources.

Robitaille et al. (2008) defined a color criterion to identify intrinsically red sources using data from the *Spitzer*-IRAC bands. Intrinsically red sources satisfy the condition $m_{4.5} - m_{8.0} \geq 1$, where $m_{4.5}$ and $m_{8.0}$ are the magnitudes in the 4.5 and 8.0 μm bands, respectively. On the other hand, an externally reddened

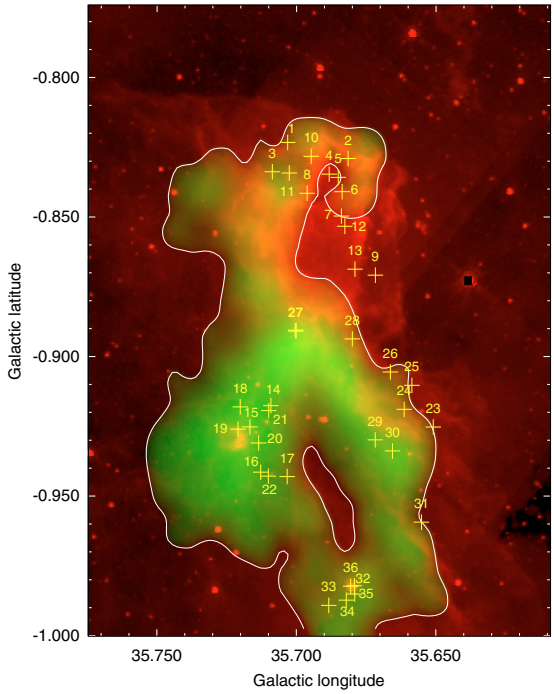

Fig. 6. Two-color image: the ^{13}CO emission integrated between 53 and 61 km s^{-1} is presented in green, and the 8 μm emission, in red. For sharper contrast, the ^{13}CO emission scale is displayed in square root and bordered by a white contour. The yellow crosses indicate the position of the intrinsically red sources, i.e., sources satisfying the condition $m_{4.5} - m_{8.0} + \varepsilon \geq 1$. We labeled the sources that appear to be related to the molecular gas around G35.6.

source is a source that is not intrinsically red (such as main-sequence stars) but appears red because of interstellar effects. They satisfy the condition $m_{4.5} - m_{8.0} < 1$ and their spectral energy distributions (SEDs) are well fitted by stellar photosphere models with interstellar extinction. To consider the errors in the magnitudes, we use a color criterion to select intrinsically red sources given by $m_{4.5} - m_{8.0} + \varepsilon \geq 1$, where $\varepsilon = \sqrt{(\Delta_{4.5})^2 + (\Delta_{8.0})^2}$ and $\Delta_{4.5}$ and $\Delta_{8.0}$ are the errors in the 4.5 and 8.0 μm bands, respectively. In Fig. 6, we show the distribution of the sources extracted from the GLIMPSE catalog around G35.6 that satisfy the previous criterion (we considered only sources with detections in both of the 4.5 and 8.0 μm bands). The intrinsically red sources are distributed into four groups. The first group (group 1) is found towards the north and includes the sources from 1 to 13. A second group (group 2) of sources is located over the south-eastern molecular structure. This portion of the molecular cloud is far from G35.6 and probably not being perturbed by the HII region. Sources 23, 24, 25, 26, 29, and 30 form group 3, which appears in the molecular gas to be likely associated with the border of the radio continuum source NVSS 185938+020012. We then identify a fourth group (group 4) towards the southern portion of the molecular cloud, far from the HII regions. Finally, sources 27, 28, and 31 are not part of any group. Sources 27 and 28, taking into account their position, could be related to the G35.6 southern border. In Table 2, we report the fluxes of the intrinsically red sources in the 2MASS and *Spitzer*-IRAC bands, specifying the GLIMPSE designation (Col. 2) and the 2MASS photometric quality (Col. 3). In the case of sources 8, 15, 19, 20, 21, 27, and 30, we derived their fluxes at 24 μm from the MIPS image and present these in Col. 11 of the table.

Table 2. Near- and mid-IR fluxes of the sources satisfying the condition $m_{4.5} - m_{8.0} + \varepsilon \geq 1$ around G35.6.

Source	GLIMPSE Desig.	2MASS Qual.	J (mag)	H (mag)	K_S (mag)	3.6 μm (mag)	4.5 μm (mag)	5.8 μm (mag)	8.0 μm (mag)	24 μm (Jy)
YSO 1	G035.7031-00.8232	BAA	16.513	14.154	12.967	12.086	11.603	11.258	10.285	
YSO 2	G035.6814-00.8290	AAA	15.830	13.625	12.495	11.284	10.692	10.049	9.182	
YSO 3	G035.7086-00.8337	BAA	16.641	13.712	12.405	11.423	11.343	10.609	10.009	
YSO 4	G035.6882-00.8346	UUA	18.264	15.119	14.434	12.445	11.992	11.545	10.877	
YSO 5	G035.6850-00.8358	UAA	17.304	15.046	13.740	12.101	11.557	11.057	10.513	
YSO 6	G035.6836-00.8409	UAE	18.038	15.025	13.485	11.546	11.054	10.487	9.958	
YSO 7	G035.6838-00.8496	UAA	17.579	15.185	14.077	12.942	12.344	12.307	11.169	
YSO 8	G035.6961-00.8415	N/A				13.176	11.297	9.674	8.558	0.14
YSO 9	G035.6716-00.8708	AAA	15.493	13.459	12.624	11.955	11.845	11.431	10.973	
YSO 10	G035.6947-00.8282	N/A				13.616	13.762		9.994	
YSO 11	G035.7025-00.8342	N/A				14.065	13.908		9.828	
YSO 12	G035.6826-00.8533	N/A				14.114	13.431		10.776	
YSO 13	G035.6790-00.8687	N/A				13.970	13.690		10.811	
YSO 14	G035.7094-00.9176	N/A				13.583	13.145	11.983	11.299	
YSO 15	G035.7166-00.9252	AAA	15.776	13.607	12.112	10.110	9.568	8.992	8.213	0.05
YSO 16	G035.7127-00.9414	AAA	15.713	14.113	13.148	11.797	11.196	10.718	10.142	
YSO 17	G035.7032-00.9430	N/A				13.242	12.489	11.977	11.313	
YSO 18	G035.7201-00.9180	N/A				14.267	15.532	12.876	11.596	
YSO 19	G035.7209-00.9260	UAA	18.218	14.992	13.379	10.983	9.856	9.109	8.363	0.16
YSO 20	G035.7135-00.9309	UUA	18.257	16.988	13.519	11.184	10.301	9.740	9.235	0.05
YSO 21	G035.7099-00.9193	N/A					13.787	12.354	11.781	0.03
YSO 22	G035.7103-00.9428	UAA	16.441	14.637	13.419	12.754	12.716	11.904	11.944	
YSO 23	G035.6509-00.9252	AAA	15.825	13.779	12.688	12.018	11.926	11.673	10.935	
YSO 24	G035.6613-00.9189	UAA	17.288	14.442	13.061	12.238	11.995	11.687	11.049	
YSO 25	G035.6585-00.9103	UAA	18.328	15.205	13.736	12.791	12.505	12.328	11.523	
YSO 26	G035.6663-00.9055	UAA	17.509	13.978	12.464	11.240	11.208	10.885	10.344	
YSO 27	G035.7002-00.8907	UUA	14.254	12.706	13.451	10.951	9.755	8.856	8.321	0.14
YSO 28	G035.6799-00.8936	UAA	17.204	15.356	14.118	13.152	12.933		10.466	
YSO 29	G035.6717-00.9298	N/A				13.379	12.823		11.280	
YSO 30	G035.6655-00.9338	N/A				14.952	13.166	11.493	11.337	0.04
YSO 31	G035.6551-00.9593	AAA	16.315	14.103	13.002	12.365	12.317	12.050	11.254	
YSO 32	G035.6791-00.9821	UAA	15.364	14.161	12.039	10.210	9.916	9.250	8.524	
YSO 33	G035.6883-00.9891	BAA	16.607	14.877	14.225	13.284	13.150		11.873	
YSO 34	G035.6820-00.9873	UAA	17.289	14.683	13.584	11.714	11.025	10.649	10.107	
YSO 35	G035.6790-00.9851	UUB	18.284	15.686	14.581	11.914	10.942	10.260	9.520	
YSO 36	G035.6804-00.9823	UAA	14.186	11.459	9.535	7.425	6.711	5.985	4.827	

Notes. The numbers of YSO candidates correspond to the numeration in Fig. 6. 2MASS Qual.: A and B are the best photometric qualities, with a $SNR \leq 10$ and ≤ 7, respectively. E means that the source magnitude is questionable. And U means that the magnitude value is an upper limit.

We identified the intrinsically red sources located in the molecular gas around the HII region G35.6. However, according to Robitaille et al. (2008) intrinsically red sources may include YSOs, planetary nebulae (PNe), galaxies, AGNs, and AGB stars. We had to apply an additional constraint to these sources to discern their real nature. Regarding extragalactic sources, Robitaille et al. (2008) pointed out that at most 0.4% of the intrinsically red sources selected by the color criterion $m_{4.5} - m_{8.0} > 1$ are galaxies and AGNs. Hence, there is a low probability of finding an extragalactic source in our small sample of red sources. To identify AGB stars, we searched in catalogues of these stars. In the region analyzed in this work, no AGB star was catalogued. To search for YSOs and PNe candidates, we constructed a color–color (CC) diagram [5.8]–[8.0] versus [3.6]–[4.5] with the sources from Table 2 that have flux detections in the four *Spitzer*-IRAC bands. We used the photometric criteria of Allen et al. (2004) to identify class I and II YSOs (Fig. 7). From their positions in this color–color diagram, we found that only source 22 cannot be classified as either a class I or II YSO. Source 30 falls outside the class I region but if we take into account the errors in the fluxes we should consider it as a YSO candidate. On the other hand, sources 7 and 18 are found in the CC diagram close to the locations of PNe, which typically have [5.8]–[8.0] > 1.4 (Cohen et al. 2007). However, we will consider them as YSO candidates too.

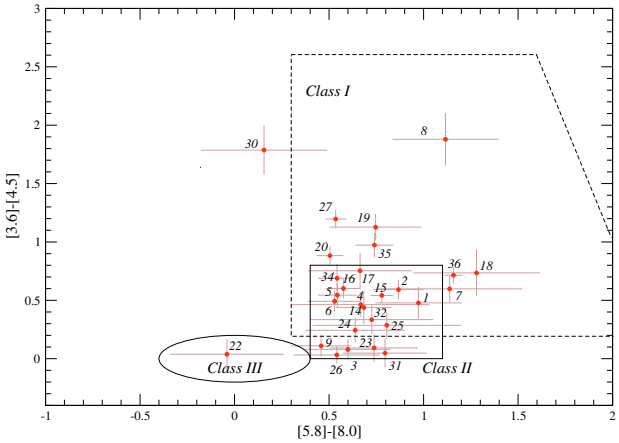

Fig. 7. Color-color diagram [5.8]–[8.0] versus [3.6]–[4.5] for sources of Table 2 with detections in the four *Spitzer*-IRAC bands. The regions indicate the stellar evolutionary stage based on the photometric criteria of Allen et al. (2004).

Finally, we fitted the spectral energy distribution (SED) of the sources from which we obtained fluxes at 24 μm from the MIPS image using the tool developed by Robitaille et al. (2007) available online[3]. We assume an interstellar absorption between

[3] http://caravan.astro.wisc.edu/protostars/

Table 3. Parameters derived from the SED fitting of sources from which we obtained fluxes at 24 μm from the MIPS image.

Source	$\chi^2_{\rm YSO}/N$	$\chi^2_\star/N$	n	$M_\star$ ($M_\odot$)	$M_{\rm disk}$ ($M_\odot$)	$M_{\rm env}$ ($M_\odot$)	$\dot{M}_{\rm env}$ ($M_\odot$/yr)	Stage
YSO 8	1	520	12	1–4	1×10^{-3}–2×10^{-1}	5×10^{-8}–3×10^{1}	0–3×10^{-4}	I
YSO 15	0.4	50	109	3–5	1×10^{-5}–1×10^{-1}	6×10^{-9}–2	0–2×10^{-7}	II
YSO 19	1	>9999	7	4	3×10^{-3}–5×10^{-2}	2×10^{-4}–8×10^{-2}	0–9×10^{-6}	I, II
YSO 20	28	>9999	1	5	3×10^{-4}	4×10^{-6}	0	II
YSO 21	0.1	505	72	0.2–5	6×10^{-4}–3×10^{-1}	9×10^{-3}–2×10^{2}	2×10^{-6}–9×10^{-4}	I
YSO 30	1.5	580	12	2–13	2×10^{-3}–5×10^{-1}	2–5×10^{2}	5×10^{-5}–6×10^{-3}	I
YSO 27	1.3	>9999	2	8–18	0–4×10^{-2}	7×10^{1}–2×10^{2}	8×10^{-5}–2×10^{-3}	I

12 and 22 mag. These values were obtained from the 2MASS *J-H* versus *H-Ks* color–color diagram (not presented here) constructed with the sources with the highest photometric quality (AAA) within a circle of 8′ in radius centered on G35.6. The lower value is compatible with the expected extinction towards star-forming regions, which, according to Neckel & Klare (1980), is generally greater than 10 mag. The upper value agrees with the visual absorption of $A_v \sim 20$ mag obtained from $A_v = 5\times10^{-22}N$(H) (Bohlin et al. 1978), where N(H) = N(HI) + $2N(H_2)$ is the line-of-sight hydrogen column density towards this region, which is about 4×10^{22} cm^{-2}. This value was obtained from both the HI column density derived from the VGPS HI data and the H_2 column density inferred by the ^{13}CO J = 1–0 data.

The SED good fitting models are selected according to the condition $\chi^2 - \chi^2_{\rm YSO} < 2N$, where $\chi^2_{\rm YSO}$ is the χ^2 of the YSO best-fit model and N is the number of input data fluxes (fluxes specified as upper limit do not contribute to N). Hereafter, we refer to models satisfying the above equation as "selected models". The fitting tool also fits the data to a stellar photosphere and defines the parameter $\chi^2_\star$ to evaluate the goodness of the fitting. By comparing $\chi^2_{\rm YSO}$ with $\chi^2_\star$ we can confirm which sources are YSOs and which sources may be stars externally reddened by the ISM. The SED fitting allows us to establish the evolutionary stage of the YSO candidates by considering the physical parameters of the sources: the central source mass $M_\star$, the disk mass $M_{\rm disk}$, the envelope mass $M_{\rm env}$, and the envelope accretion rate $\dot{M}_{\rm env}$. According to Robitaille et al. (2006): stage I YSOs are those that have $\dot{M}_{\rm env}/M_\star > 10^{-6}$ yr^{-1}, i.e., protostars with large accretion envelopes; stage II are those with $M_{\rm disk}/M_\star > 10^{-6}$ and $\dot{M}_{\rm env}/M_\star < 10^{-6}$ yr^{-1}, i.e., young objects with prominent disks; and stage III are those with $M_{\rm disk}/M_\star < 10^{-6}$ and $\dot{M}_{\rm env}/M_\star < 10^{-6}$ yr^{-1}, i.e., evolved sources whose flux is dominated by that of the central source.

In Table 3, we report the main results of the fitting output for the YSO candidates from which we obtained fluxes at 24 μm from the MIPS image. In Cols. 2 and 3, we report the χ^2 per data point of the YSO and stellar photosphere best-fit model, respectively, and in Col. 4 the number of models satisfying the χ^2 equation. The remaining columns report the physical parameters of the source, specifying the range of values of the selected models, i.e., the central source mass, disk mass, envelope mass, and envelope accretion rate, respectively. Following the criteria of Robitaille et al. (2006), the last column indicates the evolutionary stage inferred by inspecting the selected models. Figure 8 shows the SED of these sources. From this analysis, we can appreciate that for source 15 the flux at longer wavelengths originates mainly in the disk, indicating that it is a class II YSO, in coincidence with its position in the Spitzer-IRAC CC diagram. The SED for source 20 also shows the characteristics of a class II YSO. In the case of source 19, the selected models indicate that this source could be stage I and II. For sources 8, 21, 27, and 30, the selected models are those of stage I and the SED shows that the flux at longer wavelengths is dominated by the envelope flux. These sources, together with source 19, are located in the region of a class I YSO in the CC diagram (except for source 21, which lacks flux at 3.6 μm), confirming their youth.

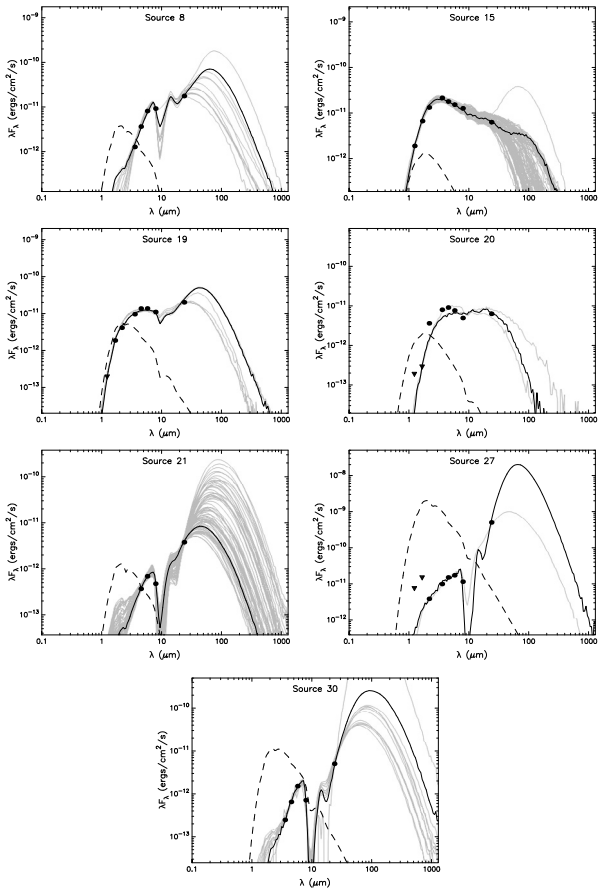

Fig. 8. SED of sources from which we obtained fluxes at 24 μm from the MIPS image. The sources are numbered according to Table 3 and Figs. 6 and 7. In each panel, black line shows the best fit, and the gray lines show subsequent good fits. The dashed line shows the stellar photosphere corresponding to the central source of the best-fit model, as it would look in the absence of circumstellar dust. The points are the input fluxes.

From Fig. 7 and the SED analysis, we can confirm the presence of YSOs around G35.6. Thus, we conclude that the region is indeed active in star formation and suggest that the birth of

some YSOs, mainly those belonging to group 1 and sources 27 and 28 may have been triggered by the expansion of the HII region G35.6. Most of the remaining intrinsically red sources belonging to groups 2, 3, and 4 may also be YSOs but their position far from the HII region does not allow us to confirm that their formation was triggered by G35.6.

8. Collect and collapse scenario

To determine whether the collect and collapse mechanism is responsible for the star formation taking place in the periphery of the HII region G35.6, we estimate and compare the age of the HII region and the fragmentation time predicted by the theoretical models of Whitworth et al. (1994a,b).

Using a simple model described by Dyson & Williams (1980), we calculate the age of the HII region at a given radius R as

$$t(R) = \frac{4\,R_{\rm s}}{7\,c_{\rm s}}\left[\left(\frac{R}{R_{\rm s}}\right)^{7/4} - 1\right],$$

where $c_{\rm s}$ is the sound velocity in the ionized gas ($c_{\rm s} = 10\,{\rm km\,s^{-1}}$) and $R_{\rm s}$ is the radius of the Strömgren sphere given by $R_{\rm s} = (3N_{\rm uv}/4\pi n_0^2\alpha_B)^{1/3}$, where $\alpha_B = 2.6 \times 10^{-13}$ cm^3 s^{-1} is the hydrogen recombination coefficient to all levels above the ground level, $N_{\rm uv}$ is the total number of ionizing photons per unit of time emitted by the star(s), and n_0 is the original ambient density.

Taking into account the results of Sect. 6, we consider a Lyman continuum photon flux of 1.0×10^{48} ph s^{-1}. Adopting a radius of ∼1.5′ for the HII region, a distance of 3.7 kpc, and an original ambient density of $\sim(1 \pm 0.5) \times 10^3$ cm^{-3}, we derive a dynamical age of between 0.18 and 0.35 Myr for G35.6. To coarsely estimate the original ambient density (assuming an error of 50%), we distribute the above calculated mass of the molecular shell, $\sim 10^4\ M_\odot$, over an ellipsoid of revolution with semiaxes of 3 and 7 pc that encloses the molecular and ionized gas.

As analyzed in Sect. 5, the morphology of the molecular gas that encircles the HII region suggests that the expansion of G35.6 collects the gas at its periphery. Finally, we ask whether the fragmentation of the collected layer of material can occur in the region. To answer this, we estimate when the fragmentation of the collected layer should occur according to Whitworth's models. Assuming a turbulent velocity in the collected layer $a_{\rm s}$ ranging between 0.2 and 0.6 km s^{-1} (Whitworth et al. 1994b), a Lyman continuum photon flux of 1.0×10^{48} ph s^{-1}, and the previously estimated original ambient density of $\sim(1 \pm 0.5) \times 10^3$ cm^{-3}, we find that the fragmentation process in the periphery of G35.6 should occur between 1.6 and 5.3 Myr after its formation, a later point in time than the G35.6 dynamical age derived above. The range in the fragmentation time is inferred by considering the error in the original ambient density and the range in turbulent velocity. Thus, we conclude that the formation of the YSOs lying at the border of the HII region most probably results from other processes, such as the radiative driven implosion (RDI) mechanism, which consists of interactions of the ionization front with pre-existing condensations (Lefloch & Lazareff 1994), or small-scale Jeans gravitational instabilities in the collected layer.

9. Summary

Using multiwavelength surveys and archival data, we have studied the ISM towards the HII region G35.673-00.847 (G35.6). This work is part of a systematic study that we are performing to increase observational evidence of triggered star formation in the surroundings of HII regions. The main results can be summarized as follows:

(a) The PAH emission around G35.6 seen at 8 μm shows that the HII region has an almost semi-ring like shape with a cut towards the Galactic west. The radius of this semi-ring is about 1.′5. The 24 μm emission reveals the presence of hot dust in the interior of the HII region.

(b) The radio continuum emission indicates that towards the south of G35.6, also identified as NVSS 185929+020334, lies the radio source NVSS 185938+020012, which is probably another HII region. From the HI absorption analysis, we conclude that both sources are located at the same distance, and from the central velocity of the related molecular gas, we estimate that the whole complex is at the kinematic distance of ∼3.7 kpc.

(c) Using the ^{13}CO J = 1–0 transition, we analyzed the molecular gas around G35.6. We identified a molecular shell composed of clumps distributed around the HII region, suggesting that its expansion is collecting the material. The molecular shell has a density of about 10^4 cm^{-3}.

(d) From a photometric study and a SED analysis, we discovered several sources (YSO candidates) very likely embedded in the molecular shell.

(e) We have presented some indirect evidence of location and properties of the exciting star(s) of G35.6 and NVSS 185938+020012. In the case of G35.6, from the radio continuum flux, the near-IR photometry, and the physical location of the analyzed sources, we find four candidates, likely O-type stars, to be the ionizing agent of the HII region. Among them, two are located close to the maximum of the 24 μm emission, and one of them (our source #6) appears to be within a hole of 5.8 μm emission, implying that it is the most likely candidate. In the case of NVSS 185938+020012, we suggest that the exciting star(s) should be later than an O9.5V star.

(f) Analyzing the HII region G35.6 dynamical age and the fragmentation time of the molecular shell surrounding the HII region, we exclude collect and collapse being the mechanism responsible for the YSO formation. We propose other possible processes of formation, such as radiative-driven implosion and/or small-scale Jeans gravitational instabilities in the collected layer.

Acknowledgements. We wish to thank the anonymous referee whose comments and suggestions have helped to considerably improve the paper. S.P. is member of the *Carrera del investigador científico* of CONICET, Argentina. A.P. and M.O. are doctoral and postdoctoral fellows of CONICET, Argentina, respectively. This work was partially supported by Argentina grants awarded by UBA, CONICET and ANPCYT.

References

Allen, L. E., Calvet, N., D'Alessio, P., & et al. 2004, ApJS, 154, 363
Bohlin, R. C., Savage, B. D., & Drake, J. F. 1978, ApJ, 224, 132
Chaisson, E. J. 1976, in Frontiers of Astrophysics, 259
Cohen, M., Parker, Q. A., Green, A. J., et al. 2007, ApJ, 669, 343
Condon, J. J., Cotton, W. D., Greisen, E. W., et al. 1998, AJ, 115, 1693
Deharveng, L., Zavagno, A., & Caplan, J. 2005, A&A, 433, 565
Dyson, J. E., & Williams, D. A. 1980, Physics of the interstellar medium (New York: Halsted Press), 204
Elmegreen, B. G., & Lada, C. J. 1977, ApJ, 214, 725
Fazio, G. G., Hora, J. L., Allen, L. E., et al. 2004, ApJS, 154, 10
Fich, M., Blitz, L., & Stark, A. A. 1989, ApJ, 342, 272
Gail, H., & Sedlmayr, E. 1979, A&A, 76, 158
Inoue, A. K. 2001, AJ, 122, 1788

Inoue, A. K., Hirashita, H., & Kamaya, H. 2001, ApJ, 555, 613
Jackson, J. M., Rathborne, J. M., Shah, R. Y., et al. 2006, ApJS, 163, 145
Kolpak, M. A., Jackson, J. M., Bania, T. M., Clemens, D. P., & Dickey, J. M. 2003, ApJ, 582, 756
Lefloch, B., & Lazareff, B. 1994, A&A, 289, 559
Lockman, F. J. 1989, ApJS, 71, 469
Martins, F., & Plez, B. 2006, A&A, 457, 637
Martins, F., Schaerer, D., & Hillier, D. J. 2005, A&A, 436, 1049
Neckel, T., & Klare, G. 1980, A&AS, 42, 251
Petriella, A., Paron, S., & Giacani, E. 2010, A&A, 513, A44
Pomarès, M., Zavagno, A., Deharveng, L., et al. 2009, A&A, 494, 987
Reich, W., Fuerst, E., Haslam, C. G. T., Steffen, P., & Reif, K. 1984, A&AS, 58, 197
Rieke, G. H., & Lebofsky, M. J. 1985, ApJ, 288, 618
Robitaille, T. P., Whitney, B. A., Indebetouw, R., Wood, K., & Denzmore, P. 2006, ApJS, 167, 256
Robitaille, T. P., Whitney, B. A., Indebetouw, R., & Wood, K. 2007, ApJS, 169, 328
Robitaille, T. P., Meade, M. R., Babler, B. L., et al. 2008, AJ, 136, 2413
Simon, R., Jackson, J. M., Clemens, D. P., Bania, T. M., & Heyer, M. H. 2001, ApJ, 551, 747
Stil, J. M., Taylor, A. R., Dickey, J. M., et al. 2006, AJ, 132, 1158
Werner, M. W., Roellig, T. L., Low, F. J., et al. 2004, ApJS, 154, 1
Whitworth, A. P., Bhattal, A. S., Chapman, S. J., Disney, M. J., & Turner, J. A. 1994a, A&A, 290, 421
Whitworth, A. P., Bhattal, A. S., Chapman, S. J., Disney, M. J., & Turner, J. A. 1994b, MNRAS, 268, 291
Zavagno, A., Pomarès, M., Deharveng, L., et al. 2007, A&A, 472, 835